Journal of the Indian Chemical Society 102 (2025) 101729

Contents lists available at ScienceDirect

Journal of the Indian Chemical Society

journal homepage: www.journals.elsevier.com/journal-of-the-indian-chemical-society

Optical, structural, electronic, and population analysis of WO_3 – Bi_2O_3 system for emerging and electrical applications

M. Hamici [a], Faisal Katib Alanazi [b,*], T. Chihi [c], M. Fatmi [c,**], M.A. Ghebouli [d]

[a] Laboratory of Dosing, Analysis and Characterization with High Resolution (DAC-hr), Ferhat Abbas-Setif1 University, Setif, 19000, Algeria
[b] Department of Physics, College of Sciences, Northern Border University, P.O. Box 1321, 91431, Arar, Saudi Arabia
[c] Research Unit on Emerging Materials (RUEM), University Ferhat Abbas of Setif 1, Setif, 19000, Algeria
[d] Department of Chemistry, Faculty of Science, University of M'sila, University Pole, Road Bourdj Bou Arreiridj, 28000, M'sila, Algeria

ARTICLE INFO

Keywords:
Molecular structure
CASTEP
WO_3–Bi_2O_3 system
Band structure
GGA-PBESOL

ABSTRACT

Phase relations in the system Bi_2O_3-WO_3 were studied. Six intermediate WO_3, Bi_2WO_6, α-Bi_2O_3, $Bi_2W_2O_9$, Bi_6WO_{12} and $Bi_3W_2O_{10.5}$ phases were investigated using density functional theory (DFT). The stability of phases in the ground state electronic DOS, elastic and the optical properties are reported. All elastic constants of all compounds, according to our calculations and in any type of crystalline cell, whether monoclinic, orthorhombic or tetragonal of the WO_3–Bi_2O_3 system, are mechanically unstable. We notice that all the compounds retained its metallic character at the fermi level, except for WO_3 and $Bi_3W_2O_{10.5}$ which represent gaps. Reflectivity, absorption, conductivity, loss energy function, real and imaginary part of the dielectric function and refractive index for WO_3 and α- Bi_2O_3 compounds are calculated with wavelength l (nm). We deduce that WO_3 and α-Bi_2O_3 are sensitive in the ultraviolet region. The optical conductivity in the real and imaginary, confirms that WO_3 is a semiconductor.

1. Introduction

A phase diagram is a graphical representation that shows the phase composition and structure of an alloy as functions of temperature and concentration at constant pressure. It is chosen to facilitate understanding of the phenomena studied and to determine phase transformations during and under heating conditions. Christopher et *al.* [1] investigated the Bismuth-rich phases in the Bi_2O_3–Nb_2O_5, Bi_2O_3–Ta_2O_5, Bi_2O_3–MoO_3 and Bi_2O_3–WO_3 systems, using synchrotron X-ray diffraction and electron diffraction, to resolve outstanding problems concerning phase relationships, unit cells, and symmetry. Our investigation focused on Bismuth-rich phases within the Bi_2O_3–Nb_2O_5, Bi_2O_3–Ta_2O_5, Bi_2O_3–MoO_3 and Bi_2O_3–WO_3 systems. We utilized synchrotron X-ray diffraction and electron diffraction techniques to address unresolved issues related to phase relationships, unit cells, and symmetry.

WO_3–Bi_2O_3 alloys have garnered significant interest due to their notable mechanical properties and technological relevance in fields such as engineering and electronics. The phase diagram of the WO_3–Bi_2O_3 system, shown in Fig. 1, was established by A.P. Finlayson [2]. However, numerous properties, including phase stabilities and electronic and mechanical characteristics, of the WO_3–Bi_2O_3 alloys remain to be comprehensively understood at the atomic level. Employing ab initio calculations based on density functional theory, this study presents a detailed analysis of the ground-state structural, electronic, and optical properties of WO_3–Bi_2O_3 alloys. Transition metals are *d*-block elements, which gradually fill an electronic *d* sub-shell below a saturated *s* sub-shell. Transition metals can form ions with a wide variety of oxidation states. The physical and chemical properties of transition metals directly influence their uses (all conductors of electricity). Transition metals are very important from an economic and social point of view due to their many applications. Transition metals generally have a high density as well as a high melting and vaporization temperature. These properties come from the ability of electrons in the *d* sub-shell to delocalize into the metal lattice. In metallic substances, the greater the number of electrons shared between the nuclei, the greater the cohesion of the metal. Tungsten W, in period 6, is also a transition metal. It has the highest melting point of all pure metals. Tungsten is the chemical element, symbol W, it is a transition element, used in the composition of many catalysts (sulphide, chloride, organometallic derivatives). Tungsten compounds are used in glasses, paints and ceramics. Tungsten has

* Corresponding author.
** Corresponding author.
E-mail addresses: Faisal.katib.al@gmail.com (F.K. Alanazi), fatmimessaoud@yahoo.fr (M. Fatmi).

https://doi.org/10.1016/j.jics.2025.101729
Received 26 September 2024; Received in revised form 23 March 2025; Accepted 22 April 2025
Available online 23 April 2025

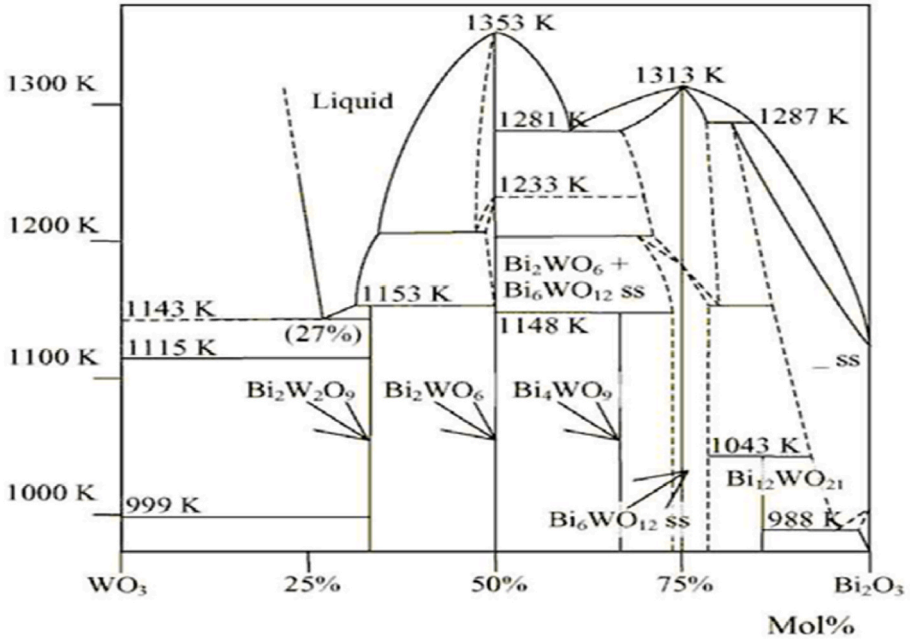

Fig. 1. The phase diagram of the WO_3– Bi_2O_3system [2].

the highest melting point of all the pure metals at 3680 °C and the second highest all over the periodic table after carbon; it is used in many high-temperature applications such as aerospace and arc welding process etc. It electrical resistivity of 5.56 10^{-8} Ω m, it is used in electrodes, and electron microscopes, used also as an interconnect material in integrated circuits. The modulus of elasticity at 25 °C of 405 10^3 N/mm^2. The tungsten has an excellent shielding property. Tungsten (W) an important transition metal, in the equilibrium state exists in two polymorphic forms: the cubic structure (Im-3m, N° 229) in more stable form β-W and the cubic A15 structure (Pm-3n, N° 223) α-W, metastable, it can coexist with the α phase at ambient conditions. The bismuth (Bi) is the chemical element with atomic number 83. It is weakly studied unlike that of other close heavy metals. The simple body Bi is a silver-white semimetal, of rhombohedral lattice or trigonal crystal system. Most chemists nevertheless consider it a heavy metal; it has the lowest electrical and thermal conductivity of all solid metals. Its thermal conductivity is about fifty times lower than that of silver (429 W/mK). Its melting point is 271.4 °C and its boiling point is 1560 °C ± 5 °C. Oxygen is the chemical element with atomic number 8, symbol O. Dioxygen with the chemical formula O_2 consists of two oxygen atoms linked by a covalent bond. Oxygen is a nonmetal that very easily forms compounds, including oxides, with virtually all other chemical elements. Oxygen is an essential component of the molecules found in all living beings: amino acids and sugars. An oxide is defined as a chemical compound made up of oxygen with another chemical element that is less electronegative than itself. $PbTiO_3$ perovskite's oxides have been investigated by Muhammad Yaseen et al. [3] using DFT and by PB sol-GGA and under pressure, showed that $PbTiO_3$ is a semiconductor up to 40 GPa. Mehwish K et al. [4] and by the first principles calculation predicted the phase stability, optical and magneto-electronic of $MAlO_3$(M = Co, Pr) perovskite's oxides compounds and confirmed that the stability of MAlO3(M = Co, Pr) perovskites is in cubic phase. M. Yaseen et al. [5] investigated by (FP- LAW) method, the electronic, optical and thermoelectric properties of $LaAlO_3$ pervoskite oxides compound under pressure and concluded that $LaAlO_3$ is a suitable candidate for Optoelectronic and Thermoelectric Devices. M. Yaseen et al. [6] by first-principles calculations and (FP-LAW) method studied the electronic, optical (in the range of energies from 0 to 30 GPa) and magnetic properties for perovskite oxides $PrXO_3$ (X = V, Cr) compounds, concluded that $PrVO_3$ has a metallic nature, while $PrCrO_3$ is half-metallic nature.

Oxides have a generally crystalline structure, in crystallized oxides; the bonds between atoms are partially ionic, covalent or metallic (transition metals). Tungsten trioxide (crystalline solid) is a chemical compound with the formula WO_3. The crystalline structure of tungsten trioxide depends on the temperature: it is triclinic, monoclinic, orthorhombic and tetragonal. Its most common form is monoclinicγ-WO_3 with $P2_1/c$ space group is a very common tungsten oxide phase stable at room temperature. A polycrystalline sample of $Bi_2W_2O_9$(which bismuth tungstate is formed depends on the ratio $1Bi_2O_3$. $2WO_3$) was synthetized with a quantity of Bi_2O_3 (99.99 % purity) and WO_3 (99 % purity) were ground together and reacted in air at 750 °C for 12 h and at 800 °C for 36 h with intermittent grinding. The single crystal X ray diffraction study on $Bi_2W_2O_9$ which also proposes a ground state of Pnab symmetry [7] fully consistent with our work.

Kevin et al. [8] determined the crystal structure of Bi_2WO_6 (formed from a 1:1 ratio of Bi2O3 to WO3) using Rietveld profile refinement and high-resolution time-of-flight neutron powder diffraction data. They concluded that it possesses an orthorhombic crystal structure in the $Pca2_1$ space group, with lattice parameters a = 5.43726 (2) Å, b = 16.43018 (5) Å, c = 5.458422 (2) Å, and Z = 4. Finlayson et al. [9] explored the properties of Bi–W oxides, specifically Bi2WO6 and Bi_6WO_{12} (formed from a 3:1 Bi_2O_3 to WO_3 ratio), using X-ray diffraction and Raman spectroscopy to analyze their structural features, and UV–vis diffuse reflectance spectroscopy coupled with the Kubelka-Munk function to determine their optical band gaps. Bismuth oxide Bi_2O_3 is polymorphic, existing in several stable and metastable forms. The different phases of Bi_2O_3 (α, β, ω, ε) crystallize in monoclinic networks $P2_1/c$, tetragonal P-421c [10], triclinic P-1 [11], and orthorhombic Pbnb [12]. In this study, we focused on α-Bi_2O_3. The compound $Bi_3W_2O_{10.5}$, derived from a 3/2 Bi_2O_3 to $2WO_3$ ratio (not present in the phase diagram), was synthesized using a solid-state technique [13]. Its crystal structure was determined to be in the tetragonal $I4/m$ space group, with lattice parameters a = 3839 (1) Å, c = 16 382 (5) Å, volume V = 241.41 Å^3, and Z = 4. This study provides a detailed investigation of the structural, electronic, mechanical, and optical properties of six intermediate phases in the WO_3–Bi_2O_3 system using density functional theory (DFT). The findings reveal that all phases are mechanically unstable, regardless of their crystalline structure, highlighting a key challenge for their

Table 1
Space groups, lattice parameters in Å, conventional volumes Å^3, number of cell formula of compounds, density in g/cm^3, energy in GPa and elastic constants in GPa in the WO_3– Bi_2O_3 system.

Compound	WO_3	$Bi_2W_2O_9$	Bi_2WO_6	Bi_6WO_{12}	α-Bi_2O_3	$Bi_3W_2O_{10.5}$
a	5.3339 (7.306)	5.2363 (5.4334)	5.499 (5.436)	11.7199 (12.510)	7.1029 (5.849 - 22.2)	3.6161 (3.839)
b	5.3339 (7.540)	5.5357 (5.4132)	5.916 (5.456)	11.7199 (12.510)	5.6333 (8.164–22.2)	3.6161 (3.839)
c	8.1521 (7.692)	24.5875 (23.6902)	16.587 (16.416)	11.3608 (11.240)	12.0751 (7.504 −22.2)	16.0907 (16.382)
Energy (eV)	−1507	−8322	−6457	−102007	−4996.5	−6504
Z	4	4	4	4	4	4
Volume	231.054 (224.132)	712.716	539.6472 (487.63)	1560.48	4 082 031	210.407 (242.4)
Space group	$P2_1/c$ (N°14)- monoclinic	*Pnab* (N°60)- orthorho.	$Pca2_1$ (N°29)- orthorho.	*I4/1* (N°80)- tetragonal	$P2_1/c$ (N°14)- monoclinic	*I4/m* (N°87)- tetragonal
Density	6.66494 (7.270)	8.8129	8.58881 (9.50)	9.466553	7.58191	9.17297
C_{ij}	unstable	unstable	unstable	unstable	unstable	$C_{11=}$ 23, $C_{33=}$ 26 $C_{44=}$ - 25, $C_{66=}$ 17 $C_{12=}$ 18, $C_{13=}$ 38 $C_{16=}$ −0.16
[Ref.]	[22]	[23]	[9]	[24]	[25]	[14]

optimization. Electronically, all compounds exhibit metallic behavior except for WO_3 and $Bi_3W_2O_{10\cdot5}$, which show band gaps, indicating potential semiconductor applications. Optical analysis demonstrates that WO_3 and α-Bi_2O_3 are highly sensitive to UV radiation, enhancing their interest for optoelectronic applications. Mulliken and Hirshfeld charge analyses reveal strong bonding interactions, particularly in $Bi_3W_2O_{10\cdot5}$. These results open new avenues for developing high-performance optical and electronic materials.

2. Computational details

For our Density Functional Theory (DFT) calculations, we utilized the CASTEP code (version 7.0) [14]. Norm-conserving pseudopotentials [15] were employed for our GGA + PBE calculations. Our approach included adopting a plane-wave basis set to represent the Kohn-Sham orbitals. After conducting convergence studies, the cutoff energy was set at 300 eV. Similarly, the Monkhorst-Pack grid was optimized, and a 4 × 4 × 4 k-point mesh was chosen as it provided well-converged results without excessive computational demand. These choices were made to balance precision and efficiency, ensuring that the structural, electronic, and optical properties were accurately captured. The justification for these parameters will be clearly stated in the revised manuscript [16]. To optimize structures, we focused on minimizing total energy. The structures under consideration were WO3 (monoclinic, $P2_1/c$, No. 14), 4Bi2W2O9 (orthorhombic, Pnab, No. 60), Bi2WO6 (orthorhombic, $Pca2_1$, No. 29), Bi6WO12 (tetragonal, I4/1, No. 80), Bi2O3 (monoclinic, $P2/c$, No. 14), and Bi3W2O10.5 (tetragonal, $I4/m$, No. 87). These were optimized through plane-wave DFT calculations using the GGA + PBE functional [17–19]. The valence electron configurations considered were W: [Xe] 4f14 5d4 6s2, Bi: [Xe] 4f14 5d10 6s2 6p3, and O: [He] 2s2 2p4. Optimization was achieved using the Broyden-Fletcher-Goldfarb-Shenno (BFGS) minimization technique to attain the most stable structure locally. The self-consistent convergence conditions were set as follows: total energy less than 0.2 × 10^{-4} eV/atom, force on each atom less than 0.05 eV/Å, offset tolerance below 0.002 Å, and stress bias under 0.1 GPa.

3. Results and discussion

3.1. Structural properties

The compounds in the WO3–Bi2O3 system are summarized in Table 1 together with their optimized and experimental structural data. Strong agreement between the calculated and actual results lays the groundwork for future assessments of the electrical and optical characteristics of these materials to be reliable. But according to our calculations, all compounds have mechanically unstable elastic constants, regardless of whether they have monoclinic, orthorhombic, or tetragonal crystalline cells (Fig. 2). For stable structures, the elastic constants need to meet the mechanical stability criterion: [20] the monoclinic and tetragonal system criteria are: $C_{11} > 0$, $C_{22} > 0$, $C_{33} > 0$, $C_{44} > 0$, $C_{55} > 0$, $C_{66} > 0$, $C_{44}C_{66} - 2C_{46} > 0$, $C_{11} + C_{22} + C_{33} + 2(C_{12} + C_{13} + C_{23}) > 0$, $C_{22} + C_{33} - 2C_{23} > 0$ and $C_{11} > 0$, $C_{33} > 0$, $C_{44} > 0$, $C_{66} > 0$, $C_{11}–C_{12} > 0$, $C_{11} + C_{33} - 2C_{13} > 0$, $2C_{11}+C_{33}+2C_{12}+4C_{13} > 0$ respectively [21]. the orthorhombic system criteria are: $C_{ii}>0$; $C_{ii} + C_{jj} - 2C_{ij} > 0 C_{11} + C_{22} + C_{33} + 2(C_{12} + C_{13} + C_{23}) > 0$. Notably, the elastic constants of Bi3W2O10.5 in its tetragonal structure, fail to meet the stability criteria of $C16 < 0$ and $C44 < 0$.

Calculating the thermodynamic stability of the compounds studied, based on their binary composition in Bi2O3 and WO3, is of interest. The enthalpy calculation is as follows:

$$xBi_2O_3 + yWO_3 \rightarrow Bi_{2x}W_yO_{3x+3y} + \Delta_{formation}H^0 \quad (1)$$

The following were the conventional formation enthalpies for the binary oxides WO_3(s) and Bi_2O_3(s): These values, which are obtained from [26,27], are ΔHo (Bi_2O_3(s), 298.15 K) = −907. 97 J.mol-1

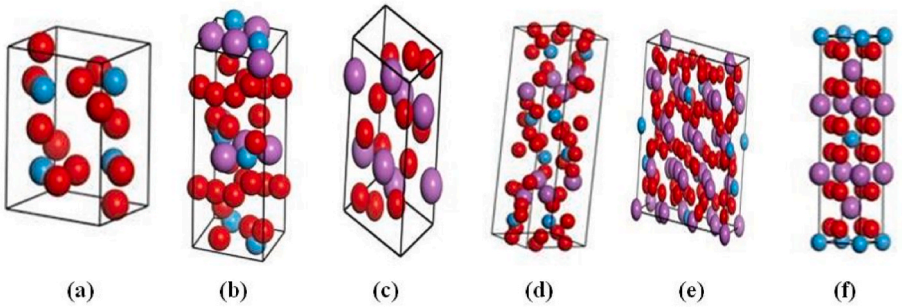

Fig. 2. Presents views of perspectives of WO_3 (a), Bi_2WO_6(b), α-Bi_2O_3 (c), $Bi_2W_2O_9$ (d), Bi_6WO_{12} (e) and $Bi_3W_2O_{10.5}$ (f) phases, respectively.

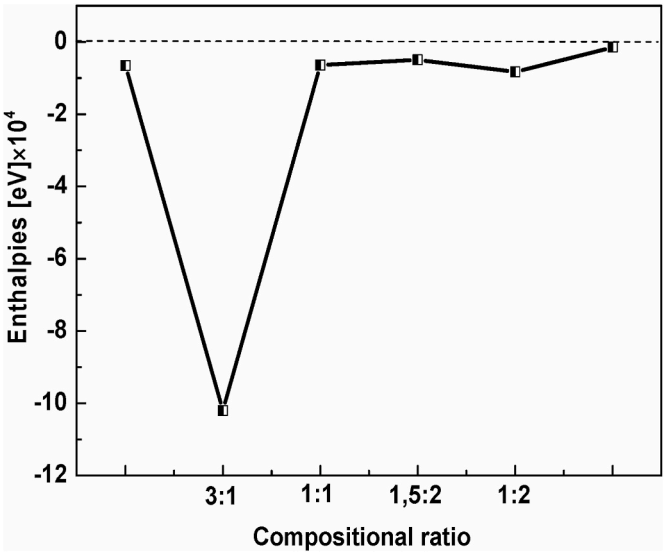

Fig. 3. The enthalpies dependence of the compositional ratio for WO_3, $Bi_2W_2O_9$, Bi_2WO_6, Bi_6WO_{12}, $Bi_3W_2O_{10.5}$ and α-Bi_2O_3 based on the Bi_2O_3/WO_3 ratios.

equivalent to (−5661 eV) and −73. 12 j. mol^{-1} equal to (-4556 eV) respectively. The enthalpies of WO_3, $Bi_2W_2O_9$, Bi_2WO_6, Bi_6WO_{12}, $Bi_3W_2O_{10.5}$, and α-Bi_2O_3 during their respective ground-state phases are displayed in eV in Fig. 3 To validate the theory that states that the total of the ratios of the entropies of the binary oxides equals the entropy of mixed oxides. We tested with the entropy of the mixed oxide $SrBi_2O$ found experimental equal to S° (298.15 K) = 206.1 ± 1.1 J K^1 mol^{-1} [28, 29]. The entropy calculated for this compound as the sum of the basic binary oxides is as follows: S° (cal) (298.15 K) = 206.7 J K^1 mol^{-1}, the value is in good agreement with that found experimentally.

3.2. Electronic properties

Our calculations indicate that in the entire energy range, all the compounds are predominantly, the valence and the conduction band are formed predominately from overlap of oxygen 2*p*-like states as seen universally in other ab initio electronic structure calculations [30] and from photoemission spectroscopy [31] with minor contributions from (W, Bi, O)-*s* states.

Specifically, WO_3 is primarily dominated by O-*p* states. The analysis of the band structure, density of states (DOS), and electronic properties provides comprehensive insights into the electronic characteristics of these materials. Using the FP-LAPW method, we calculated the energy band structure, as well as the total and partial DOS of the WO_3–Bi_2O_3 system. It was observed that all compounds maintained their metallic nature at the Fermi level, except for WO_3 and $Bi_3W_2O_{10.5}$. The band gap of WO_3 was calculated to be around 0.68 eV, which is very small compared to the experimental value. This is a common problem with the GGA functional, which strictly underestimates the band gap calculations [32]. It was found that the experimental band gap is close to 2eV.The band structures, including both total and partial DOS for WO_3, $Bi_2W_2O_9$, Bi_2WO_6, Bi_6WO_{12}, $Bi_3W_2O_{10.5}$, and α-Bi_2O_3, are depicted in Fig. 4. This figure illustrates the Fermi levels with a vertical dotted line at zero energy in the DOS. Fig. 4 also presents the total and projected local DOS for several compounds, including WO_3, $Bi_2W_2O_9$, Bi_2WO_6, Bi_6WO_{12}, $Bi_3W_2O_{10.5}$, and α-Bi_2O_3. Notably, there are two common features in the DOS profiles of these compounds.

3.3. Optical properties

In this work, the study of optical properties focuses exclusively on the fundamental compounds WO3 and α-Bi2O3 within the WO3–Bi2O3 system. By examining the optical properties, both theoretical and empirically derived, of WO3 and α-Bi2O3 crystals, we gain valuable insights into their electronic structures.

To do this, consider different photon energies to calculate some optical properties of hexagonal crystals of WO_3 and α-Bi_2O_3. We started by calculating the dielectric function ε (ω) described by its real part and its

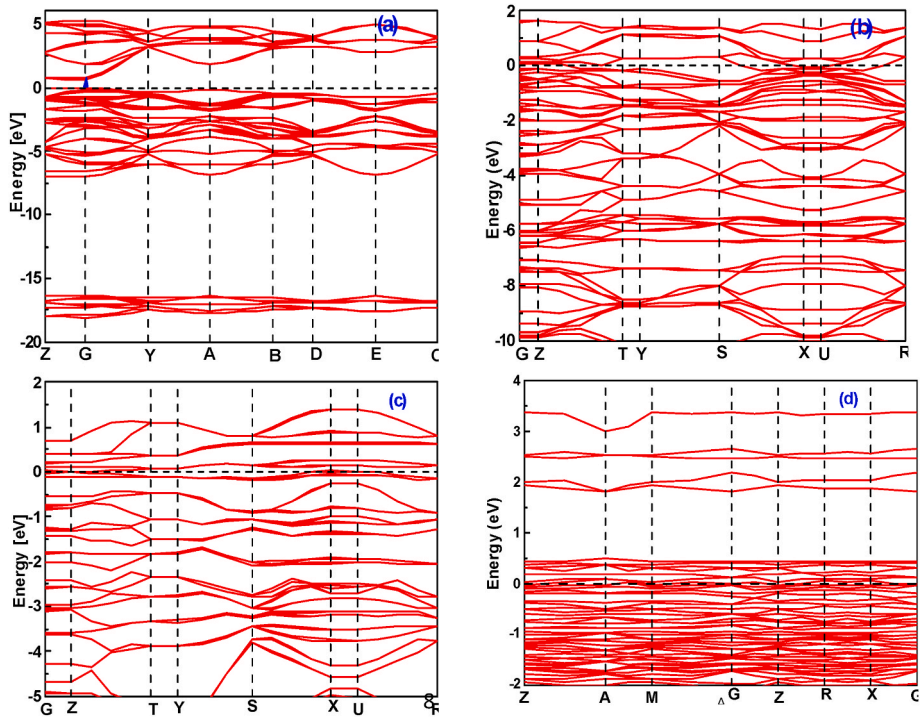

Fig. 4. Band structures, and total and partial DOS of WO3**(a)**, 2W2O9 **(b)**, Bi2WO6**(c)**, Bi6WO12 **(d)**, Bi3W2O10.5 **(e)**, and α-Bi2O3 **(f)** phases; respectively.

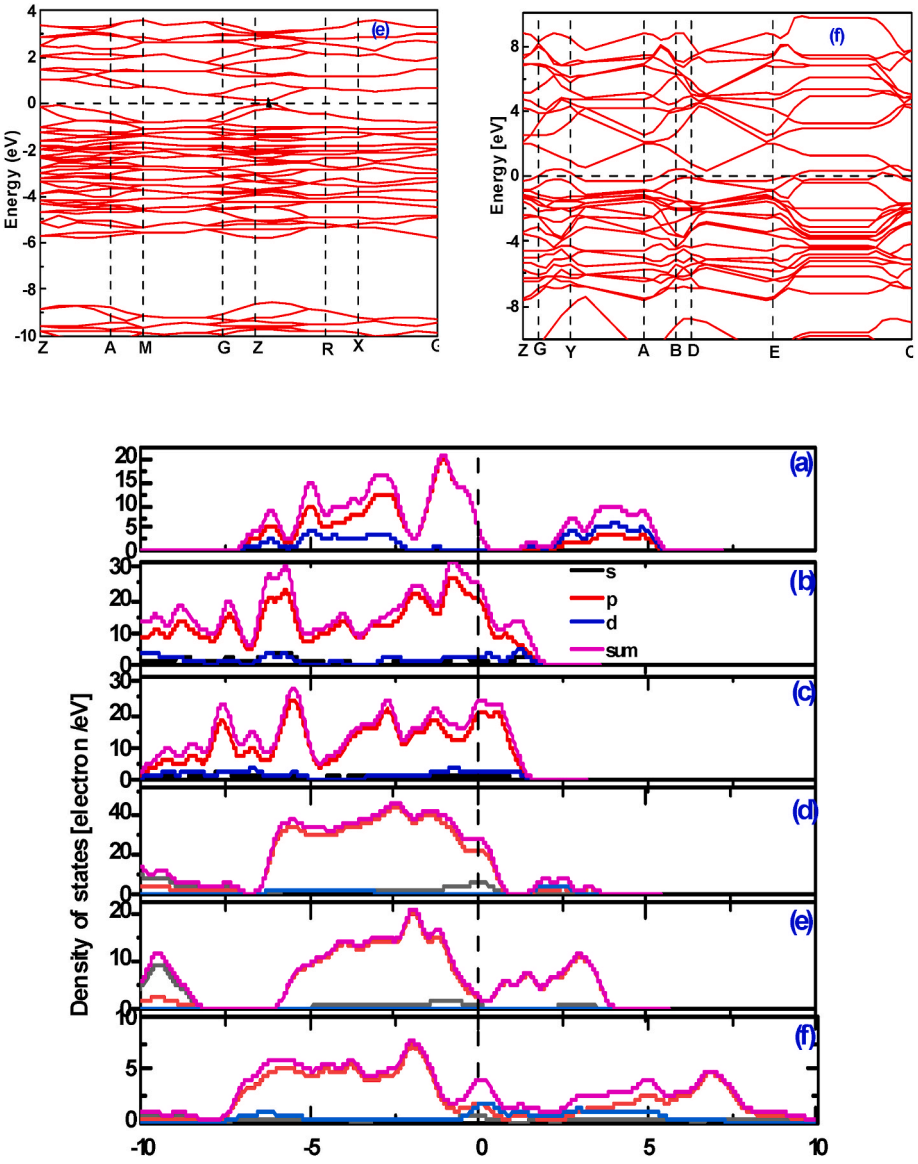

Fig. 4. (*continued*).

imaginary part and given by the formula $\varepsilon(\omega) = \varepsilon_1(\omega) + i\varepsilon_2(\omega)$, under incident polarized light according to direction [100].

The dielectric function, $\varepsilon(\omega)$, is a fundamental optical parameter that describes the absorption and polarization properties of the material, where $\varepsilon_1(\omega)$ and $\varepsilon_2(\omega)$ are the real and imaginary part of the dielectric function, respectively. The imaginary part $\varepsilon_2(\omega)$ of the dielectric function $\varepsilon(\omega)$ can be obtained from the momentum matrix between the occupied and unoccupied electronic states, which is given by [33].

$$\varepsilon_2(\omega) = \frac{2\omega^2\pi}{V\varepsilon_0}\sum_{k,v,c} |<\psi_k^c|\boldsymbol{u}.\boldsymbol{r}|\psi_v^c>|^2 \delta\left(E_k^c - E_k^v - \hbar\omega\right) \quad (2)$$

where $\boldsymbol{u}$ is the vector that provides the polarization of the electric field of the incident electromagnetic radiation, V is the volume of the unit cell, e is the electronic charge, and ψ_k^c represents the wave functionof the valence (conduction) band at the wave vector k. On the other hand, the real part $\varepsilon_1(\omega)$ of the dielectric function $\varepsilon(\omega)$ is calculated from the imaginary part of $\varepsilon_2(\omega)$ according to Kramers-Kronig relations [34]:

$$\varepsilon_1(\omega) = 1 + \frac{2}{\pi}P\int_0^\infty \frac{\omega'\varepsilon_2(\omega')}{\omega'^2 - \omega^2}d\omega' \quad (3)$$

where $\boldsymbol{P}$ implies the principal value of the integral.

Through $\varepsilon_1(\omega)$ and $\varepsilon_2(\omega)$ it is possible obtain all other optical properties, including the refractive index $n(\omega)$, optical conductivity $\sigma(\omega)$, absorption coefficient $\alpha(\omega)$, reflectivity $R(\omega)$ and loss function $L(\omega)$ by the following equations [35,36]:

$$n(\omega) = \frac{1}{\sqrt{2}}\left[\sqrt{\epsilon_1^2(\omega) + \epsilon_2^2(\omega)} + \epsilon_1(\omega)\right]^{\frac{1}{2}} (6) \quad (4)$$

$$\sigma(\omega) = \frac{\omega\varepsilon_2}{4\pi} (5)$$

$$\alpha(\omega) = \sqrt{2}\omega\left[\sqrt{\epsilon_1^2(\omega) + \epsilon_2^2(\omega)} + \epsilon_1(\omega)\right]^{\frac{1}{2}} (6)$$

$$R(\omega) = \left|\frac{\sqrt{\epsilon(\omega)} - 1}{\sqrt{\epsilon(\omega)} + 1}\right|^2 \quad (5)$$

$$L(\omega) = \frac{\epsilon_2(\omega)}{\epsilon_1^2(\omega) + \epsilon_2^2(\omega)} \quad (6)$$

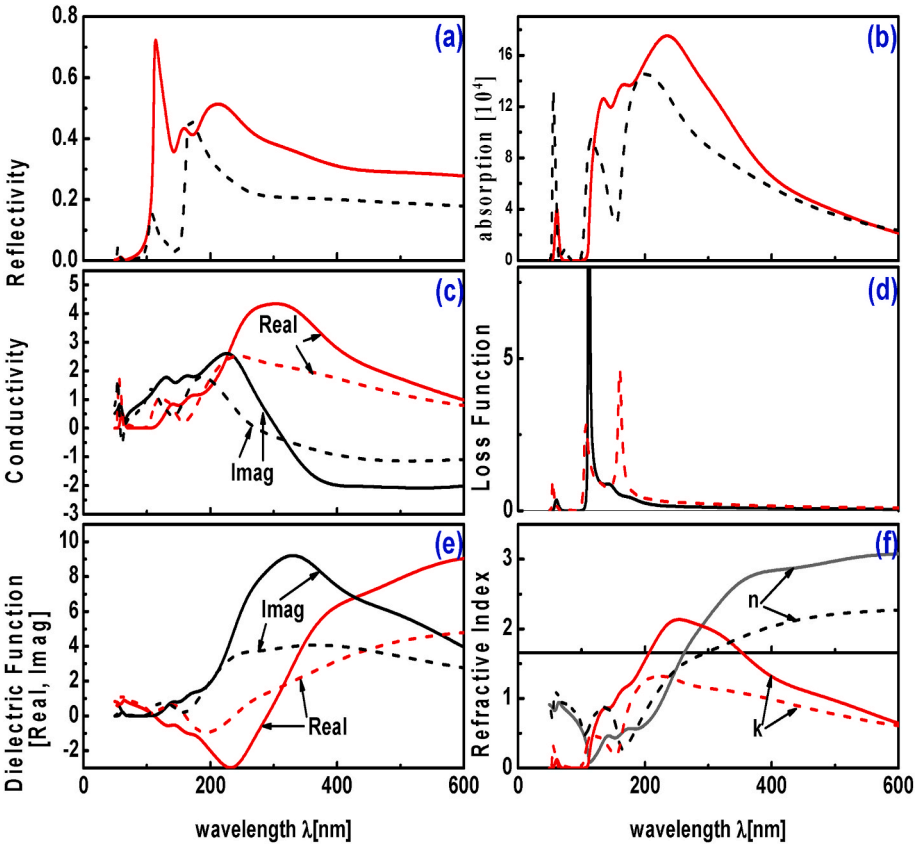

Fig. 5. Reflectivity **(a)**, absorption **(b)**, conductivity **(c)**, loss energy function **(d)**, real and imaginary part of the dielectric function **(e)** and refractive index **(f)** for the calculated compounds WO_3 and α- Bi_2O_3 (solid and dashed lines respectively with wavelength λ(nm)).

Fig. 5 displays the reflectivity, absorption, conductivity, energy loss function, and both the real and imaginary parts of the dielectric function, along with the refractive index for the compounds WO_3 and α-Bi_2O_3. A well-defined and sharp reflectance curve is obtained for the WO_3 system. The reflectivity has been found increase rapidly with increasing wavelength, reaching a maximum peak with a value about 0.7 at λ = 100 nm. Two weaker peaks appear at λ = 180 nm and λ = 200 nm. From 400 nm the reflectivity decreases sharply with increasing wavelength. On the other hand, the α-Bi_2O_3 compound presents 3 selective peaks in the UV region located at λ = 50 nm, λ = 100 nm and λ = 200 nm corresponding to maximum values of 5 %, 15 % and 50 % respectively. Beyond 400 nm in the visible region the reflectivity decreases significantly to reach less than 40 %.

As the amplitude of the reflectance increases with the increase in wavelength this can be explained by the fact that light scattering is reduced, which leads to a reduction in scattering losses and therefore a maximum reflection. The selective peaks observed is due to a loss of energies in the UV range in the dielectric structure, these values are linked to the FWHM of the peaks. This compound can help to stop dangerous ultraviolet radiation. In Fig. 5 depicts the optical absorption spectrum of the WO_3 and α-Bi_2O_3 crystals along the polarization direction [100] for the GGA approach. The peaks and valleys in the absorption curve are related to the possible transition between states in the energy bands. The absorption spectra in Fig. 5b, reveal that WO_3 and α-Bi_2O_3 are sensitive in the ultraviolet region. The optical conductivity for WO_3 and Bi_2O_3, are calculated as a function of wavelength according to Eq. (4)**.** The peaks of the real parts of the two compounds arise mainly from the interbond transitions between the occupied and unoccupied states. The optical conductivity**,** starts at λ = 51 nm in the real and imaginary part of the spectra, which confirms that WO_3 is a semiconductor. The highest optical peak with a value of 4 is obtained at λ = 300 nm, the imaginary part has a peak of 2 located at λ = 200 nm. On the other hand, the real and imaginary parts of the Bi_2O_3 compound have 3 peaks, followed by a sharp drop in the optical conductivity is observed beyond λ = 250 nm. L(ω) is an important factor describing the energy loss of a fast-moving electron in a material. The peaks in L(ω) spectrafor light polarized along the (100) plane. Fig. 5d, shows a single significant peak at λ = 120 nm for WO_3. For Bi_2O_3 and for (100) plane polarized light, there are three prominent peaks at λ = 54, 106 and 160 nm (1, 2.84 and 4.62eV) respectively. The main peak is located at λ = 160 nm, the other peaks are possibly polarized according to others not cited. These peaks correspond to the number of free electrons plasmons is the so-called plasma frequency. They represent the energy of the collective excitations of the electron charge density in the crystal, above which the material shows the dielectric behavior [$\varepsilon_1(\omega) > 0$]. From Eqs. (4) and (5), the complex dielectric constants as a function of photon energy were estimated for WO_3 and α-Bi_2O_3. The following Eq. (6) is then used to determine the complex refractive index (n and k) of WO_3 and α-Bi_2O_3 using the obtained values of the complex dielectric constants ε_1 and ε_2. The curves at λ = 600 nm are used to determine the fluctuation of the complex dielectric constant and the refractive index (a dimensionless parameter that characterizes beam propagation across that medium) of the structures WO3 and Bi_2O_3. The real part of the dielectric constant (ε_1) of WO_3 shows a dispersion with photon energy increases until it reaches a constant value of 9.04 at the same wavelength and its refractive index (n) is 3.07, compared to the static refractive index n (0) found equal to the value 1.903 with an experimental value about 1.88 [37]. The same remark is observed for the α-Bi_2O_3 structure, the real part of the dielectric constant (ε_1) is 4.76 at λ = 600 nm with a refractive index (n) of 2.27. The calculated refractive index values match very well with that obtained by another research. The line shape of n (λ) spectra is similar as ε_1 because of equations related between n and ε. The observed

Table 2
Atomic populations (Mulliken) of all electron configurations of atoms for WO_3, $Bi_2W_2O_9$, Bi_2WO_6, Bi_6WO_{12}, $Bi_3W_2O_{10.5}$ compounds.

Compounds	Bond	Population	Length (Å)	Species	s-Orbitals	p-Orbitals	d-orbitals	Total	Charge(e)	Hirshfeld charge (e)
WO_3	O–W	0.19 to 0.91	1.7765 to 2.3166	O	1.85	4.66 to 4.79	0.00	0.54 to 0.64	−0.54to −0.64	−0.22 to −0.26
	O–O	−0.07 to −0.01	2.6791 to 2.8359	W	0.27	0.16	3.76	4.19	1.81	0.74
$Bi_2W_2O_9$	O–W	0.33 to 0.78	1.36214 to 2.86409 (1.769–2.150) [23]	O	1.64to 1.97	4.42 to 4.80	0.00	6.15 to 6.68	−0.68 to -0.15	−0.35to −0.12
	W–W	−2.86 to −2.09	1.91511 to 2.62887	W	0.64	−0.36	4.97	5.26	0.74	0.46
	O–Bi	−0.61 to 0.14	1.49243 to 2.89087 (2.1816–2.5244) [23]	Bi	1.66	1.78	9.96	13.40	1.60	0.47
	Bi–Bi	−0.59	2.66770							
	O–O	−0.79 to 0.08	1.25749 to 2.97132							
Bi_2WO_6	O–O	−0.38 to 0.13	1.36355 to 2.92543	O	1.83 to 1.98	4.11 to 4.54	0.00	5.99 to 6.43	−0.43 to 0.01	−0.18 to 0.02
	O–W	0.57 to0.59	1.52276 to 1.64498	W	0.88	−0.39	5.50	6.10	−0.10	−0.04
	Bi–Bi	−0.30 to 0.64	1.91143 to 2.95237	Bi	1.64 to 1.65	2.62 to 2.70	9.98	14.24 to 14.33	0.67 to 0.76	0.27 to 0.29
	W–Bi	−1.14 to −0.46	2.01419 to 2.87571							
	O–Bi	−0.17 to 0.03	2.01922 to 2.87322							
Bi_6WO_{12}	O–W	0.44 to 0.50	1.97550 to 2.14769	O	1.89 to 1.93	4.76 to 5.10	0.00	6.68 to 6.99	−0.99 to -0.68	−0.34 to -0.24
	O–O	−0.11 to −0.02	2.06874 to 2.98246	W	0.37	0.25	3.70	4.33	1.67	0.59
	O–Bi	0.01 to 0.27	1.95720 to 2.92642	Bi	1.64 to 1.98	1.44 to 1.50	10	13.13 to 13.46	1.54 to 1.87	0.58 to 0.63
$Bi_3W_2O_{10.5}$	O–W	0.75	2.1400 (2.223) [14]	O	1.88 to 1.90	4.87 to 5.05	0.00	6.75 to 6.95	−0.75 to -0.95	−0.32 to -0.28
	O–O	−0.14 to −0.040	2.2895 to 2.8779	Bi	1.88	1.43	10.00	13.31	1.69	0.58
	O–Bi	0.10 to 0.22	2.2353 to 2.3903 (2.346–2.524)) [14]	W	0.42	0.23	3.83	4.48	1.52	0.61
α-Bi_2O_3	Bi–O	−0.07 to 0.43	1.84854 to 2.80402	O	1.83 to 1.98	4.11 to 4.54	0.00	9.92 to 9.98	−0.98 to -0.92	−0.39 to -0.35
	O–O	0.07 to −0.02	2.84782 to 2.95989	W	0.88	−0.39	9.99	13.42 to 13.74	1.26 to 1.58	0.55 to 0.57

values of dielectric constants and refraction indices for WO_3 and Bi_2O_3structures in the present work are in close agreement with the corresponding values reported by other researchers [10]. The dielectric constant values estimated in the present work are 9.04 and 4.78 for WO_3 and Bi_2O_3 respectively, which are reasonably close to the values reported by other workers [10]. It can be noted that the imaginary parts of the dielectric constants increase up to a maximum value then they decrease, the maximum values reached are 9.21 and 4.06 at $\lambda = 330$ nm and 375 nm for WO_3 and Bi_2O_3, respectively.

3.4. Population analysis

The charge density is distributed among atoms at each point, proportional to their free-atom densities relative to their distances from the nuclei. This approach results in well-localized bonded-atom distributions, each closely mirroring the molecular density around it. By integrating the atomic deformation densities (bonded minus free atoms), we define the net atomic charges and multipole moments, effectively summarizing the reorganization of molecular charge.

This permits calculation of the external electrostatic potential and the interaction energy between molecules or between parts of the same molecule [38]. The Atomic Population Analysis (specifically, Mulliken Population Analysis) of the WO3-α-Bi2O3 system compounds qualitatively describes the evolution of charge transfers and binding interactions in these homologous molecular systems (Table 2). In the WO_3-α-Bi_2O_3 system compounds, we focus on the absolute Mulliken charge values of the nearest atoms. Our interest lies in the O-(W, Bi) bonds, which exhibit the highest charge values in Bi3W2O10.5, followed by lower values in Bi_2WO_6, and even lower in Bi_6WO_{12} and $Bi_2W_2O_9$.

4. Conclusions

This study presents a comprehensive first-principles investigation of the structural, electronic, mechanical, and optical properties of six intermediate phases in the WO_3–Bi_2O_3 system using density functional theory (DFT). The findings reveal that all phases exhibit mechanical instability, indicating challenges in structural stability across monoclinic, orthorhombic, and tetragonal crystal systems. Electronic structure analysis confirms that all compounds, except WO_3 and $Bi_3W_2O_{10.5}$, retain a metallic character, suggesting selective semiconductor behavior. The optical properties indicate that WO_3 and α-Bi_2O_3 are highly sensitive in the ultraviolet region, making them promising for UV photodetectors and optoelectronic applications. Mulliken and Hirshfeld charge analyses further highlight strong bonding interactions, particularly in $Bi_3W_2O_{10.5}$. These results not only enhance the fundamental understanding of WO_3–Bi_2O_3-based materials but also pave the way for their potential use in electronic and optical device engineering. Future work could focus on experimental validation of these findings and modification strategies to improve mechanical stability.

CRediT authorship contribution statement

M. Hamici: Supervision, Software. **Faisal Katib Alanazi:** Methodology, Investigation. **T. Chihi:** Project administration, Methodology. **M. Fatmi:** Visualization, Validation. **M.A. Ghebouli:** Formal analysis.

Data availability statement

Not applicable.

Conflict of interests

NO conflicts of interest of this article.

Acknowledgement

The authors extend their appreciation to the Deanship of Scientific Research at Northern Border University, Arar, KSA for funding this research work through the project number NBU-FFR-2025-310-10.

References

[1] C.D. Ling, R.L. Withers, S. Schmid, J.G. Thompson, A review of bismuth-rich binary oxides in the systems Bi_2O_3–Nb_2O_5, Bi_2O_3–Ta_2O_5, Bi_2O_3–MoO_3, and Bi_2O_3–WO_3, J. Solid State Chem. 137 (1998) 42–61.
[2] A. Finlayson, E. Ward, V. Tsaneva, B. Glowacki, Bi2O3–WO3 compounds for photocatalytic applications by solid state and viscous processing, J. Power Sources 145 (2005) 667–674.
[3] M. Yaseen, H. Ambreen, R. Mehmood, M. Iqbal, J. Iqbal, T. Alshahrani, S. Noreen, A. Laref, Investigation of optical and thermoelectric properties of PbTiO under pressure, Physica B 615 (2021) 412857.
[4] Mehwish K. Butt, M. Yaseena, J. Iqbal, Abeer S. Altowyan, A. Murtaza, M. Iqbal, Structural, electronic, half –metallic ferromagnetic and optical properties of cubic $MAlO_3$ (M=Ce, Pr) perovskites: a DFT study, J. Phys. Chem. Solid. 154 (2021) 110084.
[5] M. Yaseen, A. Ashfaq, A. Akhtar, R. Asghar, H. Ambreen, M. Khalid Butt, S. Noreen, S. Ur Rehman, S. Bibi, S. M Ramay, A. Murtaza, Investigation of $LaAlO_3$ pervoskite compound for optoelectronic and thermoelectric devices under pressure, Mater. Res. Express 7 (2020) 015907.
[6] M. Yaseen, H. Ambreen, J. Iqbal, A. Shahzad, R. Zahid, Nessrin A. Kattan, Shahid M. Ramay, A. Mahmood, Electronic, optical and magnetic properties of $PrXO_3$(X = V, Cr): first-principle calculations, Philos. Mag. 100 (24) (2020) 3125–3140.
[7] X. Tian, Insights into the polymorphism of Bi 2 W 2 O 9: single crystal growth and a complete survey of the variable-temperature thermal and dielectric properties, CrystEngComm 20 (2018) 2669–2680.
[8] K.S. Knight, The crystal structure of russellite; a re-determination using neutron powder diffraction of synthetic Bi2WO6, Mineral. Mag. 56 (1992) 399–409.
[9] A. Finlayson, V. Tsaneva, L. Lyons, M. Clark, B. Glowacki, Evaluation of Bi–W-oxides for visible light photocatalysis, Phys. Status Solidi 203 (2006) 327–335.
[10] L. Sillen, A. Nylander, Arkiv Foer Kemi, mineralogi och geologi', 1938.
[11] L. Bourja, Étude du système CeO_2-Bi_2O_3 pour applications catalytiques et conductimétriques, ', 2011.
[12] N. Cornei, N. Tancret, F. Abraham, O. Mentré, New ε- Bi_2O_3 metastable polymorph, Inorg. Chem. 45 (2006) 4886–4888.
[13] B. Muktha, T.G. Row, Crystal structure and ionic conductivity of a new bismuth tungstate, $Bi_3W_2O_{10.5}$, J. Chem. Sci. 118 (2006) 43–46.
[14] G. Alan Sibu, P. Gayathri, T. Akila, R. Marnadu, V. Balasubramani, Manifestation on the choice of a suitable combination of MIS for proficient Schottky diodes for optoelectronic applications: a comprehensive review, Nano Energy 125 (2024) 109534.
[15] A. Arunkumar, P.M. Anbarasan, Mohd Shkir, V. Balasubramani, Computational screening of D-π-A structured with acceptor-tuned metal-free organic dye molecules for DSSCs, J. Comput. Biophy. Chem. 22 (2) (2023) 219–229.
[16] K. Periyasamy, P. Sakthivel, I. Ragavan, P.M. Anbarasan, A. Arunkumar, Mohd Shkir, C. Vidya, V. Balasubramani, Vasudeva Reddy Minnan Reddy, Woo Kyoung Kim, Design, synthesis, and optical and electrochemical properties of D–π–A type organic dyes with carbazole-based donor units for efficient dye-sensitized solar cells: experimental and theoretical studies, J. Electron. Mater. 52 (4) (2023) 2525–2543.
[17] M. El Amine Monir, A. Bendoukha Reguig, M.A. Ghebouli, K. Bouferrache, Faisal Katib Alanazi, M. Fatmi, H. Bouandas, Structural, elastic, electronic, magnetic and thermal properties of X3FeO4 (X = Mg, Ca and Sr) materials, Sci. Rep. 15 (1) (2025) 2957.
[18] W. Kohn, L.J. Sham, Self-consistent equations including exchange and correlation effects, Phys. Rev. 140 (1965) A1133.
[19] E.L. Albuquerque, U. Fulco, V. Freire, E. Caetano, M. Lyra, F. de Moura, DNA-based nanobiostructured devices: the role of quasiperiodicity and correlation effects, Phys. Rep. 535 (2014) 139–209.
[20] N. Bioud, N. Benchiheub, A. Benamrani, M.A. Ghebouli, M. Fatmi, Faisal Katib Alanazi, R. Yekhlef, Predicted thermodynamic structural and elastic properties of SrCuP and SrCuSb for thermoelectric applications, Sci. Rep. 15 (1) (2025) 4082.
[21] M.A. Ghebouli, K. Bouferrache, F.K. Alanazi, B. Ghebouli, M. Fatmi, Stability, mechanical, optoelectronic and thermoelectric behaviors of inor2025ganic metal halide double perovskites (Cs2, K2, Rb2) SnCl6: promising green energy alternatives, Solid State Commun. 397 (2025) 115831.
[22] B. Loopstra, H. Rietveld, Further refinement of the structure of WO_3, Acta Crystallogr. B 25 (1969) 1420–1421.
[23] B.J. Campbell, H.T. Stokes, D.E. Tanner, D.M. Hatch, ISODISPLACE: a web-based tool for exploring structural distortions, J. Appl. Crystallogr. 39 (2006) 607–614.
[24] W. Zhou, Defect fluorite superstructures in the Bi_2O_3-WO_3 system, J. Solid State Chem. 108 (1994) 381–394.
[25] S. Ivanov, R. Tellgren, H. Rundlo, V. Orlov, Structural studies of α-Bi_2O_3 by neutron powder diffraction, Powder Diffr. 16 (2001) 227–230.
[26] S. Phapale, R. Mishra, D. Das, Standard enthalpy of formation and heat capacity of compounds in the pseudo-binary Bi_2O_3–Fe_2O_3 system, J. Nucl. Mater. 373 (2008) 137–141.
[27] Bing-yuan Han, Andrey V. Khoroshilov, Alexander V. Tyurin, Alexander E. Baranchikov, Mikhail I. Razumov, Olga S. Ivanova, Konstantin S. Gavrichev, Vladimir K. Ivanov, WO_3 thermodynamic properties at 80–1256 K revisited, J. Therm. Anal. Calorim. 142 (2020) 1533–1543.
[28] J. Leitner, D. Sedmidubský, K. Růžička, P. Svoboda, Heat capacity, enthalpy and entropy of $SrBi_2O_4$ and $Sr_2Bi_2O_5$, Thermochim. Acta 531 (2012) 60–65.
[29] K. Popa, O. Beneš, P.E. Raison, J.C. Griveau, P. Pöml, E. Colineau, R.J.M. Konings, J. Somers, Heat capacity of Bi_2UO_6, J. Nucl. Mater. 465 (2015) 653–656.
[30] F. De Angelis, C. Di Valentin, S. Fantacci, A. Vittadini, A. Selloni, Theoretical studies on anatase and less common TiO_2 phases: bulk, surfaces, and nanomaterials, Chem. Rev. 114 (2014) 9708.
[31] R. Egdell, S. Eriksen, W. Flavell, Oxygen deficient SnO_2(110) and TiO_2(110): a comparative study by photoemission, Solid State Commun. 60 (1986) 835.
[32] F. Wang, C. Di Valentin, G. Pacchioni, Electronic and structural properties of WO_3: a systematic hybrid DFT study, J. Phys. Chem. C 115 (2011) 8345.
[33] D. Li, F. Ling, Z. Zhu, X. Zhang, Theoretical studies on the structural, electronic, and optical properties of Cu2CdGeSe4, Phys. B Condens. Matter 406 (2011) 3299–3302.
[34] Y. Fang, X. Kong, D. Wang, J. Liu, S. Cui, First principal calculations of electronic, band structural, and optical properties of BixSr1-xTiO3 perovskite, J. Phys. Chem. Solid. 127 (2019) 107–114.
[35] M. Zhong, Q.-J. Liu, C.-L. Jiang, F.-S. Liu, B. Tang, X.-J. Peng, Structural, elastic, electronic, phonon, dielectric and optical properties of Bi3TeBO9 from first-principles calculations, J. Phys. Chem. Solid. 121 (2018) 139–144.
[36] M. Jubair, A.T. Karim, M. Nuruzzaman, M. Zilani, Comparison of structural, mechanical and optical properties of tantalum hemicarbide with tantalum monocarbide: ab initio calculations, J. Phys. Commun. 3 (2019) 055017.
[37] X. Wang, L. Liu, Y. Zhang, A novel chaotic block image encryption algorithm based on dynamic random growth technique, Opt Laser. Eng. 66 (2015) 8–10.
[38] A. Tanto, T. Chihi, M.A. Ghebouli, M. Reffas, M. Fatmi, B. Ghebouli, Prediction study of structural, elastic and electronic properties of FeMP (M= Ti, Zr, Hf) compounds, Results Phys. 9 (2018) 763–770.